Solid state nuclear magnetic resonance spectroscopy as a tool to characterize natural organic matter and soil samples. The basic principles

Espectroscopía de resonancia magnética nuclear de estado sólido: una herramienta para caracterizar materia orgánica natural y muestras del suelo. Principios básicos

Pellegrino Conte [1,3,*], Alessandro Piccolo [2,3]

1. Dipartimento di Ingegneria e Tecnologie Agro-Forestali (DITAF), Università degli Studi di Palermo, v.le delle Scienze 13, 90128 Palermo, Italy

2. Dipartimento di Scienze del Suolo, della Pianta, dell'Ambiente e delle Produzioni Animali (DiSSPAPA), via Università 100, 80055 Portici (Na), Italy

3. Centro Interdipartimentale per la Spettroscopia di Risonanza Magnetica Nucleare (CERMANU), Università di Napoli Federico II, via Università 100, 80055 Portici (Na), Italy

* Email: pellegrino.conte@unipa.it

ABSTRACT:

Basic principles of solid state nuclear magnetic resonance spectroscopy (SS-NMR) are presented here. This paper is not pretending to provide an exhaustive treatment of the basics of SS-NMR. However, it will give an overview of the main applications in the characterization of environmental systems and will describe the problems related to the acquisition of quantitative solid state NMR spectra.

Keywords: Natural Organic Matter, Solid State NMR, CPMAS ^{13}C-NMR, Environmental Systems

REFERENCES AND LINKS

[1] M. A. Wilson, *NMR Techniques and Applications in Geochemistry and Soil Chemistry*, 1st ed., Pergamon Press, London (1987).

[2] P. Conte, R. Spaccini, A. Piccolo, "State of the art of CPMAS C-13-NMR spectroscopy applied to natural organic matter", *Progr. Nucl. Magn. Res. Spectr*. **44**, 215-223 (2004).

[3] A. P. M. Kentgens, "A practical guide to solid-state NMR of half-integer quadrupolar nuclei with some applications to disordered systems", *Geoderma* **80**, 271-306 (1997).

[4] D. M. Moore, R. C. Reynolds, *X-ray Diffraction and the Identification and Analysis of Clay Minerals*, 2nd ed., Oxford University Press, New York (1997).

[5] I. Kögel-Knaber, "Analytical approaches for characterizing soil organic matter", *Org. Geochem.* **31**, 609-625 (2000).

[6] E. O. Stejskal, J. D. Memory, *High Resolution in the Solid State. Fundamentals of CP/MAS*, Oxford University Press, New York (1994).

[7] M. J. Duer, *Solid-State NMR Spectroscopy: Principles and Applications*, 1st ed., Blackwell Science, Oxford, (2002).

[8] R. L. Cook, C. H. Langford, R. Yamdagni, C. M. Preston, "A modified cross-polarization magic angle spinning ^{13}C NMR procedure for the study of humic materials", *Anal. Chem.* **68**, 3979-3986 (1996).

[9] R. L. Cook, C. H. Langford, "Structural characterization of a fulvic acid and a humic acid using solid-state ramp-CP-MAS ^{13}C nuclear magnetic resonance", *Environ. Sci. Technol.* **32**, 719-725 (1998).

[10] B. Chefetz, M. J. Salloum, A. P. Deshmukh, P. G. Hatcher, "Structural components of humic acids as determined by chemical modifications and carbon-13 NMR, pyrolysis-, and thermochemolysis-gas chromatography/mass spectrometry", *Soil Sci. Soc. Am. J.* **66**, 1159-1171 (2002).

[11] K. J. Dria, J. R. Sachleben, P. G. Hatcher, "Solid-state carbon-13 nuclear magnetic resonance of humic acids at high magnetic field strengths", *J. Environ. Qual.* **31**, 393-401 (2002).

[12] R. Kiem, H. Knicker, M. Körschen, I. Kögel-Knaber, "Refractory organic carbon in C-depleted arable soils, as studied by C-13 NMR spectroscopy and carbohydrate analysis", *Org. Geochem.* **31**, 655-668 (2000).

[13] X. Y. Dai, C. L. Ping, G. J. Michaelson, "Characterizing soil organic matter in Arctic tundra soils by different analytical approaches", *Org. Geochem.* **33**, 407-419 (2002).

[14] A. Samoson, T. Tuherm, J. Past, "Ramped-speed cross polarization MAS NMR", *J. Magn. Reson.* **149**, 264-267 (2001).

[15] H. Kawashima, O. Yamada, "A modified solid-state C-13 CP/MAS NMR for the study of coal", *Fuel Process. Technol.* **61**, 279-287 (1999).

[16] P. Conte, A. Piccolo, B. van Lagen, P. Buurman, P. A. de Jager, "Quantitative aspects of solid-state ^{13}C-NMR spectra of humic substances from soils of volcanic systems", *Geoderma* **80**, 327-338 (1997).

[17] A. M. Gil, E. Alberti, "The effect of magic angle spinning on proton spin-lattice relaxation times in some organic solids", *Solid State Nucl. Mag.* **11**, 203-209 (1998).

[18] W. G. Blann, C. A. Fyfe, J. R. Lyerla, C. S. Yannoni, "High-resolution carbon-13 NMR study of solid .pi.-.pi. molecular complexes using "magic angle" spinning techniques", *J. Am. Chem. Soc.* **103**, 4030-4033 (1981).

[19] P. Conte, A. Piccolo, B. van Lagen, P. Buurman, M. A. Hemminga, "Effect of residual ashes on CPMAS-C-13 NMR spectra of humic substances from volcanic soils", *Fresen. Environ. Bull.* **10**, 368-374 (2001).

[20] U. Scheler, "Solid polymers", p. 483-511 in *Solid-State NMR Spectroscopy: Principles and Applications*, M. J. Duer Edt., 1st ed., Blackwell Science, Oxford, (2002).

[21] O. N. Antzutkin, "Sideband manipulation in magic-angle-spinning nuclear magnetic resonance", *Prog. Nucl. Mag. Res. Sp.* **35**, 203-266 (1999).

1. Introduction

Many analytical techniques have been developed for the analysis of the organic and inorganic soil constituents [1]. Among those, solid state nuclear magnetic resonance spectroscopy (SS-NMR) represents a very powerful tool to qualitatively and quantitatively characterize natural organic matter (NOM) [2] and to reveal the chemical characteristics of both amorphous and crystalline soil minerals [3].

Minerals and natural organic matter (NOM) are normally analyzed by X ray diffraction (XRD) [4] and wet chemical methods such as high performance size exclusion chromatography, pyrolysis gas-chromatography with mass spectrometry, titrations, and so on [5]. However, XRD requires high crystalline degree of minerals, whereas wet chemical analyses for NOM need sample treatments that can modify structure and conformation of the organic matter. Conversely, analyses by solid state NMR spectroscopy can be applied directly on bulk soils in order to study either unperturbed soil organic matter and amorphous minerals or the nature of the interactions between NOM and clay minerals [1].

The aim of the present paper is to provide a description of the basic principles of the NMR spectroscopy in the solid state. However, detailed information can be achieved in various details and complexity in very specialized textbooks [1,6,7].

2. The magnetic moment and the NMR phenomenon

A nucleus can be considered as a source of magnetic field ($\overline{B_N}$). The strength of $\overline{B_N}$ is measured by a vector called magnetic moment (μ) directed from the South to the North pole of the field. μ relates to a fundamental nuclear property that is the spin ($\bar{I}$) through equation (1):

$$\bar{\mu} = \frac{\gamma \bar{I} h}{2\pi} = \gamma \hbar \bar{I}\,, \qquad (1)$$

where $h = \hbar / 2\pi$ is the Planck constant, and γ is the gyromagnetic ratio that is a nuclear constant characteristic for each nucleus.

Figure 1 shows that all the magnetic moments of a population of nuclei are randomly oriented in a three-dimensional space in the absence of any magnetic field. However, when the nuclei are placed in a *z*-oriented magnetic field ($\vec{B}_0$) their magnetic moments are aligned along the direction of the applied field and spin around the *z* axis (Figure 2).

The random $\vec{\mu}$ orientation depicted in Fig. 1 is associated to a iso-energetic distribution of the nuclear spins. However, after the application of the *z*-aligned magnetic field, the energy of the nuclear spins is split to different levels according to the quantum magnetic number (m) whose values are related to I: $m = -I-n,...,-I-1,-I,I+1,...I+n$. The stronger the applied magnetic field, the larger is the difference between the nuclear spin levels (Fig. 3). The NMR phenomenon is based on the transition of the nuclear spin from the low- to the high-energy spin level.

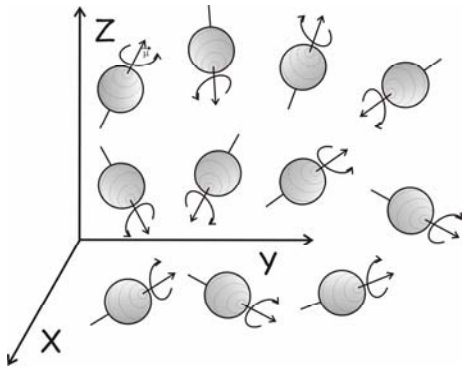

Fig. 1: Nuclear spin population randomly oriented.

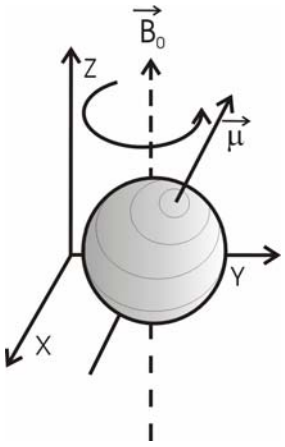

Fig. 2: Precession of the magnetic moment about an applied magnetic field.

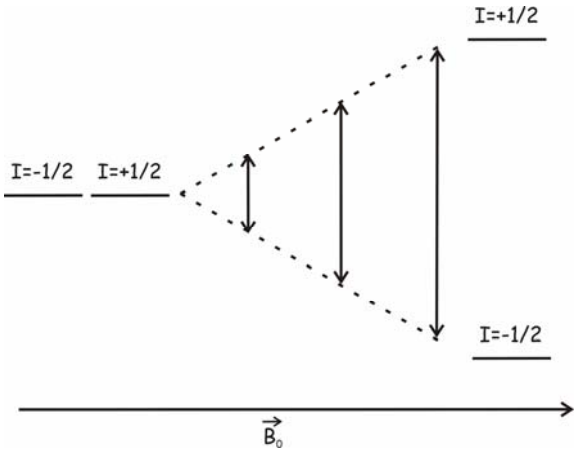

Fig. 3: Splitting of the nuclear spin levels in a *z*-oriented magnetic field for a nucleus with I=1/2.

Only nuclei having $I \neq 0$ are NMR-active (or sensitive) and can be detected. Moreover, NMR sensitivity is also directly related to γ values and to the nuclear relative abundance. In fact, the higher the γ value and the relative abundance, the larger is the NMR sensitivity of the selected nucleus. Table I reports the natural abundances (%), the spin quantum numbers and the gyromagnetic ratios of many NMR active nuclei.

According to Table I the most NMR-sensitive nuclei are ^{1}H, ^{19}F, ^{31}P, ^{27}Al, ^{23}Na and ^{55}Mn since they have either the highest isotopic relative abundance or the largest γ value.

Table I
Properties of NMR-active nuclei
(from Bruker Almanac 2005)

Nucleus	I	γ (x10^{7} rad T^{-1}s^{-1})	Natural abundance (%)
^{1}H	1/2	26.8	99.99
^{13}C	1/2	6.7	1.10
^{15}N	1/2	-2.7	0.37
^{17}O	5/2	-3.6	0.04
^{19}F	1/2	25.2	100.00
^{23}Na	3/2	7.1	100.00
^{25}Mg	5/2	-1.6	10.00
^{27}Al	5/2	7.0	100.00
^{29}Si	1/2	-5.3	4.67
^{31}P	1/2	10.8	100.00
^{55}Mn	5/2	6.6	100.00
^{113}Cd	1/2	-6.0	12.22
^{119}Sn	1/2	-10.0	8.59

3. Larmor frequency and Magnetization

The frequency of precession ($\bar{\omega}$) of the magnetic moment (also referred to as Larmor frequency) around the *z*-axis after the application of $\bar{B}_0$ is proportional to the strength of the applied magnetic field as described in equation (2):

$$\bar{\omega} = \gamma \bar{B}_0 \,. \qquad (2)$$

Since the giromagnetic ratio differs for each nucleus (Table I), the Larmor frequency is specific for each nucleus and therefore has a different value for ^{1}H, ^{13}C, ^{19}F etc.

The *z*-axis projection of the magnetic moment rotating around $\bar{B}_0$ is called magnetization ($\bar{M}$) (Fig. 4).

Compared to $\bar{\mu}$ that rotates around the *z*-axis at the Larmor frequency, the magnetization ($\bar{M}$) is unaffected by the applied magnetic field. It is used to physically describe the behaviour of the nuclei in a *z*-oriented magnetic field under the action of another magnetic field applied perpendicularly to the former one for a short period of time (the pulse). In fact, when a new magnetic field is applied along the *x* or the *y*-axis, the *z*-oriented magnetization is reversed towards the *xy*-plane. This behaviour is associated to the jump of the nuclear spin from the ground energy level to the excited one (Fig. 5).

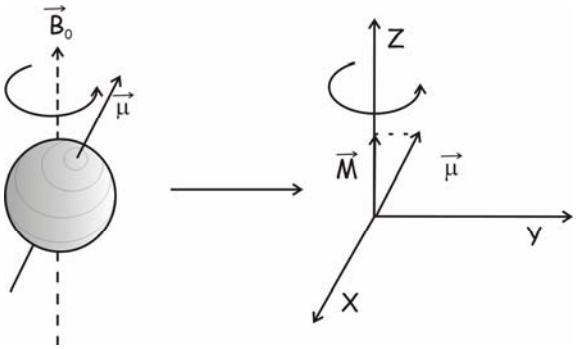

Fig. 4: Definition of the magnetization.

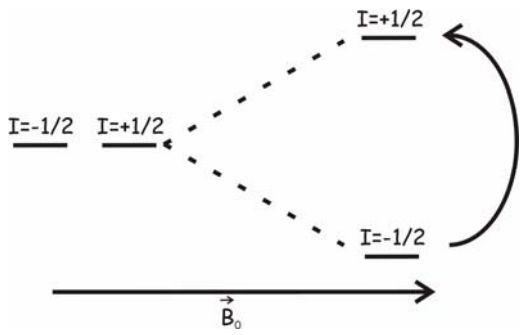

Fig. 5: Nuclear excitation due to the application of a radiofrequency pulse.

4. The fate of the magnetization after the application of the pulse

After application of a pulse followed by nuclear excitation, the nuclei relax to the ground energetic state or, in other words, the spin population returns to the equilibrium state. In terms of magnetization fate, the nuclear relaxation can be described as a precession of $\bar{M}$ around two axes: the first one is the z-axis along which $\bar{B}_0$ is aligned, whereas the second is that along which the pulse was applied (Fig. 6).

Since the mathematical treatment of the two precessional movements is very difficult, a new reference frame can be introduced. The new frame is obtained by rotating the fixed lab-frame around the z-axis at the Larmor frequency (Fig. 7A). In this way, the precessional movement around the z-axis is nulled and only that around the axis along which the pulse was applied must be mathematically treated (Fig. 7B).

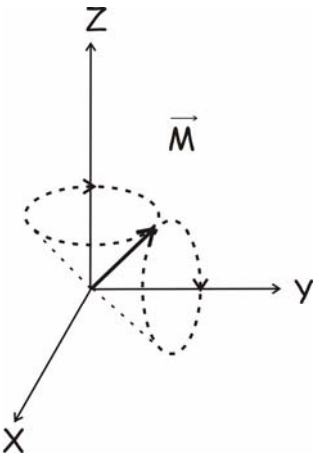

Fig. 6: Precession of the magnetization around the *z* and the *y* axes. The former is the axis along which $\bar{B}_0$ is aligned. The pulse was applied along the *y* axis.

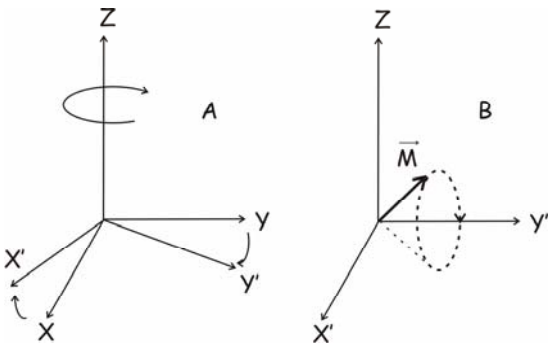

Fig. 7: A. from the static lab frame (XYZ) to the rotating frame (X'Y'Z); B. Precession of the magnetization in the rotating frame.

5. Bloch equations and free induction decay (FID)

Once the magnetization is moved from the *z*-axis, three non-null $\overline{M}$ components are generated ($M_x, M_y,$ and M_z) (Fig. 8). The fate of the three components can be vectorially described by the Bloch equations:

$$\begin{aligned}\frac{\partial M_z(t)}{\partial t} &= \gamma\left(\overline{M}(t)\times\overline{B_0}(t)\right)_z - R_1\left(M_z(t)-M_0\right)\\ \frac{\partial M_x(t)}{\partial t} &= \gamma\left(\overline{M}(t)\times\overline{B_0}(t)\right)_x - R_2 M_x(t)\\ \frac{\partial M_y(t)}{\partial (t)} &= \gamma\left(\overline{M}(t)\times\overline{B_0}(t)\right)_y - R_2 M_y(t)\end{aligned} \qquad (3)$$

where R_1 and R_2 are the spin- lattice (or longitudinal) relaxation rate and the spin-spin (or transverse) relaxation rate, respectively. M_0 is the value of the magnetization before pulse application. The rate constants R_1 and R_2 are the reciprocal of two time constants referred to as T_1 and T_2. T_1 and T_2 are defined as spin-lattice and spin-spin relaxation times, respectively.

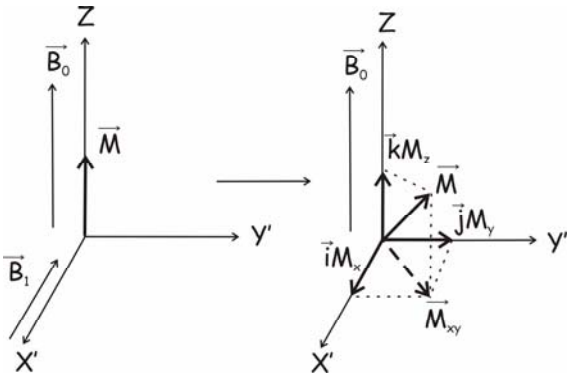

Fig. 8: Application of a pulse ($\overline{B_1}$) to generate the three components of the magnetization.

The spin-lattice relaxation rate describes the return of M_z to the initial state, whereas the spin-spin relaxation rate relates to the decay of the transverse magnetization (M_{xy}) to zero.

The Bloch equations depict the NMR signal (FID = free induction decay) as a sum of exponentially damped sinusoidal functions (Fig. 9). Each function is obtained after application of a pulse. As a consequence, NMR experiments are achieved by applying from few to hundred thousands pulses. The advantages of such experimental approach are outlined below. R_2 governs the length of time during which the FID can be observed, whereas R_1 governs the minimum time required for equilibrium to be restored.

The Bloch formulation does not provide a microscopic explanation of the origin or magnitude of the relaxation rate constants, nor is it extendible to more complex, coupled spin systems. In more complex spin systems the product operator formalism must be used to understand the NMR phenomenon [7]. This formalism will be not considered here since it is out from the aim of the present paper.

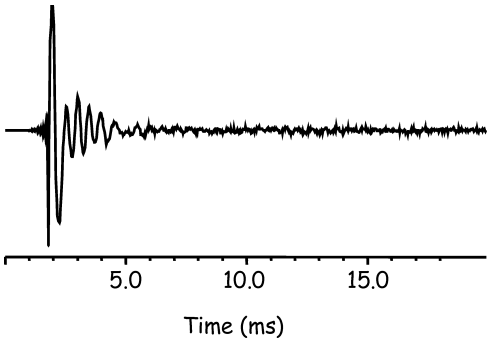

Fig. 9: Shape of a NMR signal in the time domain (FID).

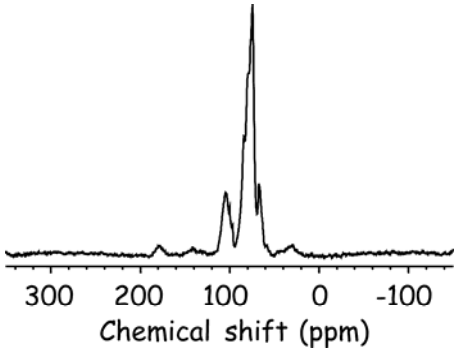

Fig. 10: Shape of a spectrum after Fourier Transformation.

6. The chemical shift

Figure 9 shows a NMR spectrum where the intensity of the signals is reported in the time domain. Since such a spectrum is difficult to read and to interpret, a Fourier transformation (FT) is applied in order to transform the time domain to the frequency domain (Fig. 10). The larger the number of pulses (*NP*) used to obtain the FID, the higher is the signal-to-noise (S/N) ratio in the Fourier transformed spectrum. In fact, there is a direct relationship between S/N and $\sqrt{NP}$. As a general rule, the ideal number of pulses to be used in a NMR experiment is that providing the best S/N ratio in a reasonable machine time. Once FT is done, the spectrum can be read in order to obtain two different information: 1. the amount of nuclei generating the signal, 2. the chemical environment of the nucleus generating the signal. Point 1. can be achieved by integration of the signal intensity, whereas point 2. can be matched by

analysing the signal position in the NMR spectra. Summarizing: NMR spectra can be used either to quantitatively estimate the amount of nuclei belonging to different functional groups or to build up molecular structures from the analysis of the spectral signal patterns. The different positions of the NMR signals in the spectra arise from the simultaneous interaction of a nucleus with an electron and of the electron with the applied magnetic field. The relationship dealing with the complex interactions between nuclei-electrons-magnetic fields can be summarized as in [3].

$$\bar{\omega} = \gamma \overline{B_0}\left(1 - \bar{\sigma}\right). \qquad (4)$$

$\bar{\sigma}$ is the shielding tensor: the larger the electron density, the stronger is $\bar{\sigma}$ thereby providing lower $\bar{\omega}$ values. Since $\omega = 2\pi\nu$, equation (4) can be re-written in scalar terms as in [4]:

$$\nu = \frac{\gamma}{2\pi} B_0\left(1 - \sigma\right). \qquad (5)$$

where ν is the chemical shift expressed in Hz.

ν is strongly dependent on the strength of the applied magnetic field. In order to obtain reproducible spectra for molecular systems analyzed on NMR devices dealing with different magnetic field strengths, the chemical shifts are expressed in ppm according to [5]:

$$\delta = \frac{\nu_S - \nu_R}{\nu_R} \times 10^6 . \qquad (6)$$

In Eq. (6) ν_S is the resonance frequency of the sample, and ν_R is the resonance frequency of a reference. The standard normally used to calibrate ^{1}H and ^{13}C NMR spectra is the tetramethylsilane (TMS, $(CH_3)_4Si$). The frequency of the carbons and that of the protons of TMS are placed at 0 ppm. Among the main properties of a NMR standard, two appear very important: 1. the reference nucleus must resonate in a chemical shift range far away from the region where the sample signals appear; 2. the standard must be easily removed in order to prevent sample contamination after NMR analysis.

7. How to depict a NMR experiment

Figure 11 graphically represents a NMR experiment. It can be divided in three main parts. The first part is called preparation. It is a waiting time between pulses to let magnetization reach the ground state after excitation. Evolution follows preparation. It is a period during which the magnetization evolves according to the interactions among nuclei. Evolution time is not always present in a NMR experiments. In fact, many experiments (such as the basic solid state ones) are thought without such a time. Finally the acquisition is the time during which the FID is recorded. At the end of the preparation period and before evolution starts, the pulses are applied. In more complicated experiments, where additional pulses are needed to obtain more detailed NMR information, an additional mixing time is placed between evolution and acquisition. However, the description of the mixing time is out of the aims of the present chapter. The reader must refer to specific literature (i.e. Ref. [7]) to deep knowledge about more complicated NMR experiments.

Fig. 11: Typical graphical representation of a NMR experiment.

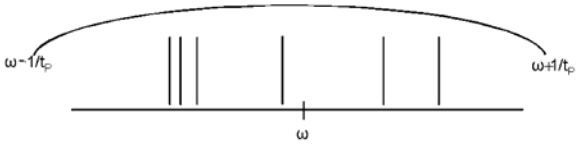

Fig. 12: Spectral width and definition of pulse length. The vertical bars represent NMR signals.

8. The pulse

In order to excite as much nuclei as possible, the pulse length must be wide enough to comprise all the spin systems in the molecules.

Equation (4) states that nuclei belonging to the same spin system (i.e. ^{1}H) do not resonate all at the same Larmor frequency ($\bar{\omega}$), but in an interval of frequencies (the spectral width, SW) depending on the $\bar{\sigma}$ value. The SW limits are $\omega \pm 1/t_P$ where t_P is the pulse length (Fig. 12). Once the nucleus to be observed is set by selecting its spectral width and its Larmor frequency (normally it corresponds to the SW center), pulse duration must be calibrated in order to include the left and right limits of the spectral width.

9. The acquisition

A FID is recorded during the acquisition time (AQ) following pulse application. In order o save disk space and to fasten NMR experiments, FIDs are not collected continuously, but sampled. The resulting points are combined to obtain the shape reported in Fig. 9.

The amount of points (time domain, TD) that are collected during FID sampling is set before each experiment. The time domain is directly related to AQ and spectral resolution: the larger TD, the higher is the spectral resolution and the longer is AQ.

In solid state NMR, TD values are limited by AQ as recommended by NMR producers.

10. Chemical shift anisotropy (CSA) and dipolar coupling

Molecules in the solid state occupy fixed positions. The molecular motions are restricted to local vibrations and rotations, whereas translational movements are inhibited by the absence of a solvent. Due to the molecular immobility, the main interactions among nuclei in the solid state are the dipolar ones.

Being I and S two different spin systems (with I the most abundant one), the dipolar interaction I→S is described by a vector connecting nucleus I to nucleus S (Fig. 13).

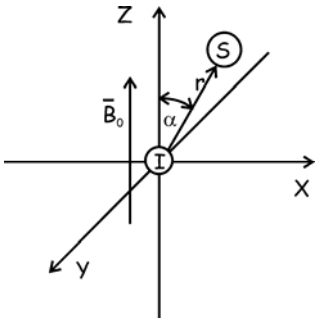

Fig. 13: The IS vector describes the dipolar interaction among two nuclei. α is the angle between the vector IS and the z-axis along which the applied magnetic field is applied. r is the length of the vector.

Relation (7) describes the dependence of the chemical shift value of the S nucleus on the orientation (α) and length (*r*) of the IS vector (Fig. 13).

$$\omega_S \propto \pm \frac{\hbar \gamma_I \gamma_S}{2r^3}(3\cos^2\alpha - 1)\,. \qquad (7)$$

The term $(3\cos^2\alpha - 1)$ is related to the chemical shift anisotropy according to which the chemical shift is not the same in all the directions. In fact, the resonance frequencies depend on the local field at the site of the resonating nucleus that varies from point to point throughout the sample due to different orientations of neighbouring nuclei. Conversely, the term $\hbar\gamma_I\gamma_S / r^3$ describes the dipole-dipole interaction (also indicated as dipolar coupling) among nuclei I and S that is related to α. The longer the distance among the two nuclei I and S, the weaker is the dipolar interaction.

According to [6], the S spin population may interact with many nearby I spins all with different relative orientations to S. For a common powder sample (all possible orientations) this means that the NMR signal appears as a broad featureless line (Fig. 14).

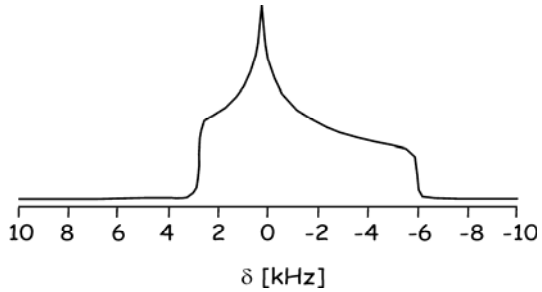

Fig. 14: Broad band generated by the resonance of a nucleus in a solid matrix. Due to the different possible orientations of the crystals, the same nucleus provides many un-resolved and overlaid NMR signals.

11. Decupling and magic angle spinning (MAS)

In order to decrease the dipolar coupling among heteronuclei and increase spectral resolution (sharper NMR signals), nucleus I may be decoupled while S is observed. Decoupling consists in the application of a train of short pulses that allows rapid transitions between the different dipolar orientations of nucleus I. For this reason nucleus S interacts with a sort of average between the states of nucleus I and the splitting of the S lines (that generates line broadening) collapses. The decoupling of the nucleus I while S is analyzed is reported in Fig. 15.

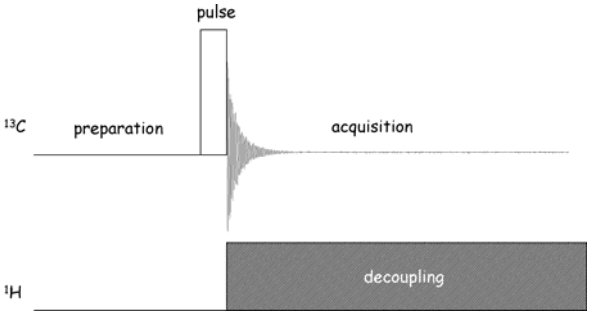

Fig. 15: Pictorial representation of the decoupling of nucleus I (i.e. ^{1}H) while nucleus S (i.e. ^{13}C) is analyzed.

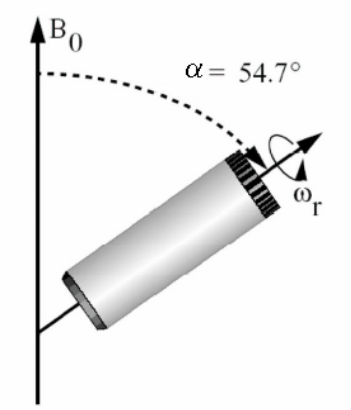

Fig. 16: Fast sample rotation around the magic angle. ω_r is the rotor spin rate.

Based on relation (7), the value of α=54.7° (the magic angle) nulls the term $(3\cos^2\alpha - 1)$, thereby reducing the line broadening caused by chemical shift anisotropy. Since dipolar interactions can be also weakened by fast rotations, a fast sample rotation around the magic angle (Fig. 16) coupled to the decoupling of I produces solid state spectra with line broadening similar to that revealed by liquid state NMR experiments.

Many problems may arise when fast sample rotation is used to acquire solid state spectra [2]. Among those, sample heating and vortex effect may reduce NMR sensitivity [2].

12. Cross polarization (CP) and Hartmann-Hahn condition

NMR sensitivity of a low-sensitive nucleus (i.e. ^{13}C) can be increased by using the cross polarization (CP) technique [2]. It is based on the excitation of the sparse spin system, S, through the abundant one, I (i.e. ^{1}H).

If the Larmor frequencies ω_I and ω_S are adjusted by varying the oscillating field amplitudes to satisfy the Hartmann-Hahn condition $\gamma_I B_{1I} = \gamma_S B_{1S}$ so that $\omega_I = \omega_S$, then a resonance exchange of energy between I and S can take place readily through a mutual spin flip mechanism [6]. The flip mechanism can be understood by using the thermal contact analogy. In fact, the Hartmann-Hahn condition can be considered as a thermal exchange between a hot system (the sparse spin S) and a cold one (the abundant I spin system). The cooling down of S is associated to the warming up of the I nuclei. The time required to reach the thermal equilibrium between I and S is called contact time (CT). Spin system I can be cooled down by application of a 90° pulse. After that, the two spin systems I and S are put in thermal contact through a pulse train having a CT duration that allows Hartmann-Hahn matching. Finally, a decoupler is switched on to decouple nucleus I while acquisition of S signals is performed (Fig. 17).

Figure 18 reports the shape of the spectra of adamantane when the sample is analyzed A. in static conditions and without decoupling, B. without MAS and with decoupling, C. with MAS and no decoupling, D. with MAS, decoupling and cross polarization.

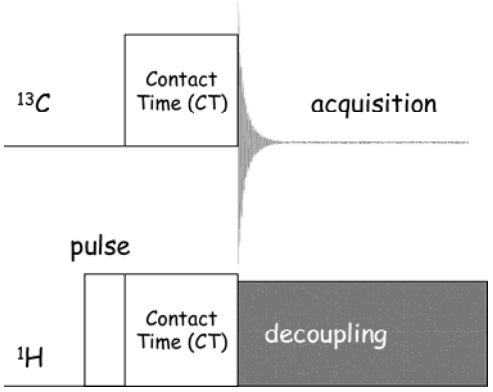

Fig. 17: Pictorial representation of a cross polarization magic angle spinning NMR experiment on carbon 13.

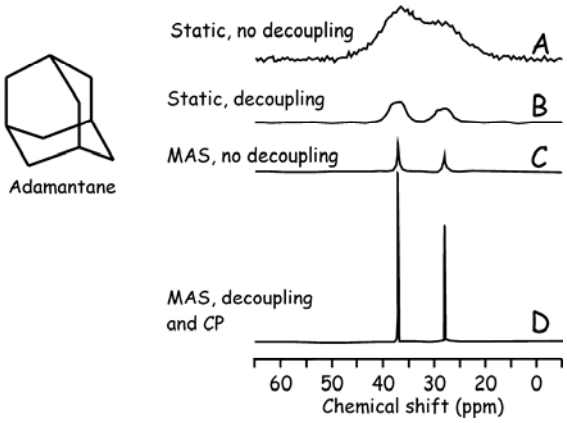

Fig. 18: Spectra of adamantane recorded in different experimental conditions. See text for details.

13. Factors affecting Hartmann-Hahn efficiency

The efficiency of the Hartmann-Hahn matching and thus the rate of cross polarization is strongly affected by the rotor spin rates (2). The rate of cross polarization depends on the strength of the dipolar interactions between I and S. The stronger the I-S coupling, the faster is the rate of magnetization

transfer. Cross polarization rates are enhanced when internuclear distances are shorter and coupling between nuclei is stronger. Anything which disrupts the coupling may slow down the cross polarization rate and lower the spectral sensitivity.

Increasing rotor spin rates has the consequence of reducing the I-S coupling, thereby providing slower cross polarization and lower NMR sensitivity.

The experimental fluctuations in cross-polarization rate, as the sample spinning rate is increased, are described for a C-H system in Fig. 19. The figure shows a typical Hartmann-Hahn spectrum of a solid adamantane sample for which the signal intensity is plotted versus the carbon radio-frequency (rf) field at a constant magnetic field of 22.6 MHz. The lower part of Fig. 19 shows that the signal intensity of a non-spinning sample reaches a plateau by varying the rf amplitude used to change B_{1C}. In this case, all rf amplitudes corresponding to the plateau can be used to match the Hartmann-Hahn condition and to obtain an efficient cross polarization between proton and carbon. Conversely, the signal intensity of the rapidly spun sample is subjected to fluctuations, as the B_{1C} amplitude varies (upper part of Fig. 19). The matching of the Hartmann-Hahn condition is thus much more difficult to achieve, since it can be reached only when B_{1C} values range in the narrow region below the maxima of the signal intensity.

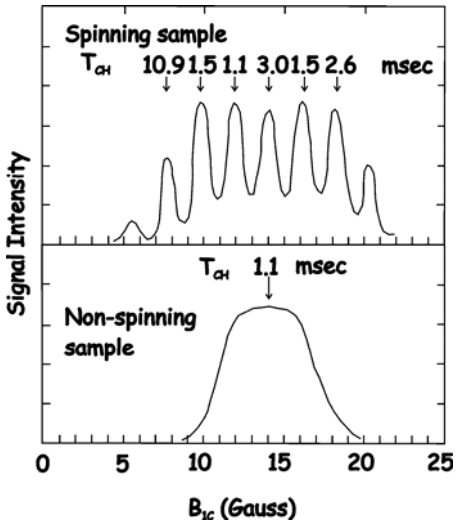

Fig. 19: Hartmann-Hahn (Ha-Ha) condition affected by fast sample rotation. The lower part of the figure shows that Ha-Ha is stable in a wide range of rf fields when samples are not spun. Upper part of the figure reports fluctuations of the Ha-Ha condition when a fast rotation is applied on the sample (adapted from reference [6]).

14. Strategies used to overcome imperfect Hartmann-Hahn matching

The difficulties in matching the Hartmann-Hahn at high fields and achieving fast rotations are simply overcome by using the single-pulse-excitation (SPE) technique reported in Fig. 15. This is also called Bloch decay (BD) or direct polarization (DP) NMR and consists of simple and very time consuming direct excitation of a nucleus S such as carbon-13.

RAMP amplitude cross polarization NMR techniques (RAMP CPMAS NMR) account for the deficiencies in Hartmann-Hahn conditions at high fields and fast rotations of protonated samples. In RAMP CPMAS NMR the amplitude of one of the rf fields (I or S spin systems) is varied during polarization transfer (Fig. 20a, b). The commonly applied RAMP CP pulse sequence for analysis of organic samples is shown in Fig. 20a. The ^{1}H rf field is increased linearly while that of ^{13}C is kept constant (^{1}H RAMP CPMAS). This sequence was used to characterize Laurentian humic and fulvic acids extracted from forest podzols [8,9] and to study peat samples [10], and several other humic substances extracted from soils of different origin [11]. ^{1}H RAMP CPMAS has also been employed on humic acids extracted from long-term agricultural experiments in Europe to investigate the refractory organic carbon remaining in arable soils [12], and to characterize humic matter from soils such as Mollisols and Gelisols [13].

An alternative ramped pulse sequence is based on a constant ^{1}H rf field and a linearly increased ^{13}C spin lock sequence (^{13}C RAMP CPMAS) [2,8,14]. The effect of the ^{13}C ramping on the cross polarization efficiency does not differ from that applied to ^{1}H [2]. Up to now, the ^{13}C RAMP CPMAS sequence has been used only by Kawashima and Yamada [15] to characterize coal samples with a high-field NMR machine and very fast sample spinning. These workers employed a ^{13}C RAMP CPMAS sequence that was somewhat different from that normally described in the literature. They stepwise decreased the ^{13}C rf field (Fig. 20b) instead of increasing it, as is commonly done [2,8,14]. To our knowledge, no works were conducted to compare the efficiency of the cross polarization with decreasing and increasing ^{13}C rf fields.

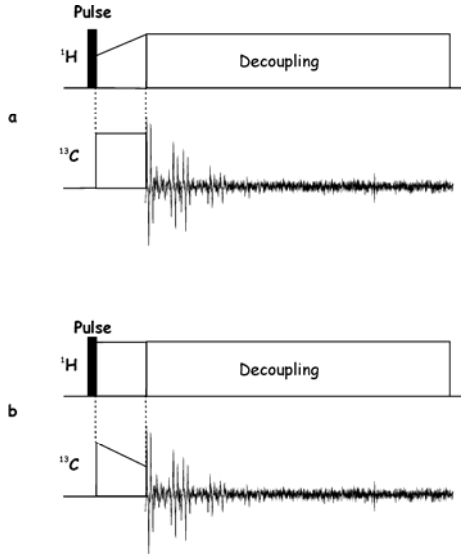

Fig. 20: a. Classical RAMP sequence with increasing amplitude of the ^{1}H rf field; b. Modified RAMP sequence with decreasing amplitude of the ^{13}C rf field.

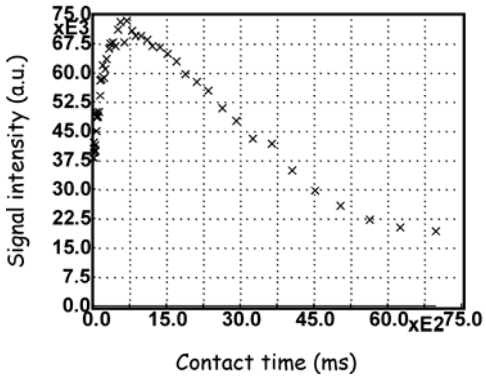

Fig. 21: Variable Contact Time profile used to measure the optimum contact times in quantitative CPMAS ^{13}C-NMR spectroscopy

15. Variable contact time experiments (VCT)

A simplified mathematical formulation describing the cross polarization in organic systems followed by nuclear relaxation is reported in equation (8):

$$I(t) = I_0\left[1-\frac{T_{CH}}{T_{1\rho}(H)}\right]^{-1}\times \exp\left(-\frac{CT}{T_{1\rho}(H)}\right)\times \left[1-\exp\left(-\frac{\left(1-\frac{T_{CH}}{T_{1\rho}(H)}\right)CT}{T_{CH}}\right)\right]. \quad (8)$$

Here T_{CH} is the cross polarization time, whereas $T_{1\rho}(H)$ is the proton spin-lattice relaxation time in the rotating frame. T_{CH} measures the time needed to reach the maximum cross polarization, whereas $T_{1\rho}(H)$ is a time constant related to the proton relaxation following their excitation with a 90° pulse. The fundamental CPMAS ^{13}C-NMR relationship that must be valid to apply equation (7) is: $T_{CH}<<T_{1\rho}(H)$.

Experimental setup where a series of NMR spectra are acquired with different CT values gives variable contact time experiments (VCT). VCT are used to measure optimum contact times (OCT) for a given organic sample. OCT is used to acquire quantitative CPMAS ^{13}C-NMR spectra of organic systems through mathematical interpolation of equation (8) (Fig. 21) [16].

16. The spin diffusion

The magnetization transfer from abundant I to scarce S nuclei in solid state NMR arises mainly from the dipolar interactions among these nuclei. As revealed by relation (7), the shorter the I-S distance (such as in the case of ^{1}H-^{13}C systems), the stronger is the dipolar interaction between the two nuclei and the faster the cross polarization, and, hence, the higher the spectral sensitivity. However, another mechanism of magnetization transfer can be observed in the solid state. This involves dipolar interactions among the abundant nuclei (i.e. ^{1}H) themselves. One I may induce spin re-orientation on any other I nucleus in the surroundings (flip-flop process), that, in turn, may then interact either with near-by S nuclei (i.e. ^{13}C) or other near-by I (Fig. 22).

The main effect of spin diffusion in natural organic matter (NOM) is that both intra- and intermolecular cross polarizations, which depend on the proton density (proton is the abundant spin system in NOM) within heterogeneous systems, become possible [16]. For this reason, quaternary carbons positioned in the proximities of regions with high proton density can become visible by CPMAS [17].

Spin diffusion through different proton distributions was used to explain differences in optimum contact time (OCT) for humic substances extracted from different pedogenetic soils [15] and to understand conformational properties of fulvic and humic acids extracted from volcanic soils [19]. Factors such as rotor spin rates, that affect heteronuclear dipolar interactions involved in the Hartmann-Hahn matching, also influence the homonuclear dipolar interactions and the spin diffusion. In particular, a fast rotor spinning speed is assumed to weaken the spin diffusion effect [20].

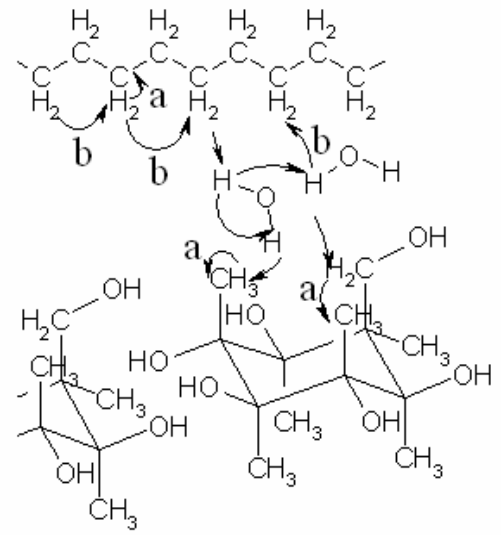

Fig. 22: Mechanisms of magnetization transfer. a. cross polarization; b. spin diffusion

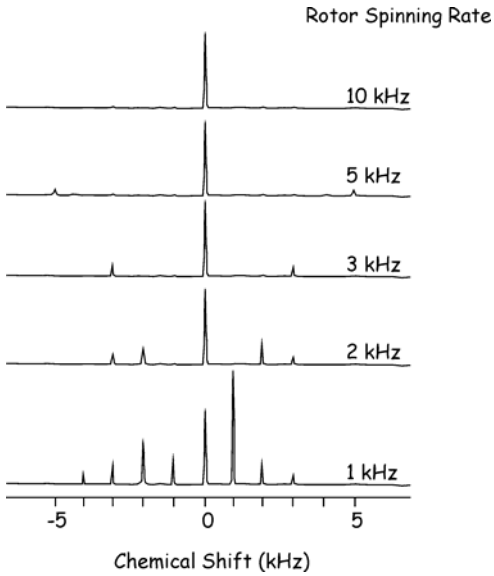

Fig. 23: Effect of fast rotation on spinning side bands (SSB). Increasing the sample spinning rate leads to decreasing of both amount and intensity of SSB (from reference [2]).

17. Spinning side bands

If the rate of sample spinning is less than the frequency of the chemical shift anisotropy, spinning side bands (SSB) may appear in CPMAS spectra in addition to the signal centered at the isotropic chemical shift [2]. SSB are positioned at chemical shifts equal to the spinning frequency at both the right and left side of the centerband, regardless of the strength of the applied magnetic field [6].

The effect of spinning rate on the number and intensities of SSB is shown in Fig. 23. The SSB can be easily recognized because their intensities decrease and their positions change as the spinning rate varies, whereas the position and intensity of the centerband remain unchanged. As shown in Fig. 23, the centerband is not necessarily the most intense signal in a spectrum with SSB.

Chemical shift anisotropy can be affected by the degree of crystallinity in amorphous materials and the content of planar groups. Side bands in CPMAS ^{13}C NMR spectra of amorphous natural organic matter are mainly due to planar carbonyl and aromatic systems. The presence of SSB may alter the qualitative and quantitative understanding of spectra, since SSB may be mistaken as signals of non-existent functional groups, and distort relative intensities of some spectral regions, thereby jeopardizing accurate quantitation of the nuclei of different carbons.

Different approaches have been suggested to suppress side bands in CPMAS ^{13}C-NMR spectroscopy. A detailed review on sideband manipulation is given by Antzutkin [21]. In particular, one of the best ways to eliminate SSB is to maximize the rotor spin velocity, i.e.: up to 15-20 kHz, and, preferably, to make use of the RAMP pulse sequence to prevent cross polarization inefficiency. Neverthless, when available NMR devices do not allow fast spinning, other options may be applied. The best method is to employ the TOSS (Total Suppression of Side Bands) pulse sequence [2]. The TOSS sequence consists of a series of four to six 180° pulses, with phase cycling to compensate for pulse imperfections, applied on the carbon-13 just before spectrum acquisition.

Although TOSS has been widely applied on natural organic matter its quantitative reliability is still unclear. Duer [2] reported that the intensities of centerbands decrease with TOSS, as compared to those obtained without TOSS. This implies that the quantitative reliability of CPMAS ^{13}C NMR TOSS experiments on natural organic matter still needs to be verified.

When the TOSS sequence is not available because of instrument limitation, a simple mathematical SSB subtraction has been suggested to account for the anisotropic signal dispersion in spectra of NOM [15]. Spinning side bands in CPMAS ^{13}C NMR spectra of NOM are mainly represented by chemical shift anisotropy of carboxyl groups, while the SSB arising from aromatic systems are in most cases low and negligible. Aliphatic chains in amorphous materials do not produce side bands. Signal areas can be corrected for these SSBs by measuring the area under each side band in the region where it is clearly visible, and subtracting this value from the

area of the region where the side band is covered by other signals. Since different carbon groups contribute to SSBs, their measured areas must be also added to the centerband area to account for the tranfer of signal to the SSBs. A limitation of such mathematical SSB subtraction may be due to an underestimation of hidden SSBs (such as those possibly given by aromatic moieties), and to the assumption that visible SSBs have the same shape and intensity as the hidden ones.

